Photoactivation mechanism of a carotenoid-based photoreceptor

Sepalika Bandara[a], Zhong Ren[a,1], Lu Lu[b], Xiaoli Zeng[a,2], Heewhan Shin[a], Kai-Hong Zhao[b,1], and Xiaojing Yang[a,c,1]

[a]Department of Chemistry, University of Illinois at Chicago, Chicago, IL 60607; [b]State Key Laboratory of Agricultural Microbiology, Huazhong Agricultural University, Wuhan 430070, China; and [c]Department of Ophthalmology and Vision Sciences, University of Illinois at Chicago, Chicago, IL 60607

Edited by Elisabeth Gantt, University of Maryland, College Park, MD, and approved May 9, 2017 (received for review January 17, 2017)

Photoprotection is essential for efficient photosynthesis. Cyanobacteria have evolved a unique photoprotective mechanism mediated by a water-soluble carotenoid-based photoreceptor known as orange carotenoid protein (OCP). OCP undergoes large conformational changes in response to intense blue light, and the photoactivated OCP facilitates dissipation of excess energy via direct interaction with allophycocyanins at the phycobilisome core. However, the structural events leading up to the OCP photoactivation remain elusive at the molecular level. Here we present direct observations of light-induced structural changes in OCP captured by dynamic crystallography. Difference electron densities between the dark and illuminated states reveal widespread and concerted atomic motions that lead to altered protein–pigment interactions, displacement of secondary structures, and domain separation. Based on these crystallographic observations together with site-directed mutagenesis, we propose a molecular mechanism for OCP light perception, in which the photochemical property of a conjugated carbonyl group is exploited. We hypothesize that the OCP photoactivation starts with keto–enol tautomerization of the essential 4-keto group in the carotenoid, which disrupts the strong hydrogen bonds between the bent chromophore and the protein moiety. Subsequent structural changes trapped in the crystal lattice offer a high-resolution glimpse of the initial molecular events as OCP begins to transition from the orange-absorbing state to the active red-absorbing state.

photoreceptor | light perception | photoprotection | carotenoid-binding protein | dynamic crystallography

Orange carotenoid protein (OCP) is a photoreceptor that regulates light harvesting and mediates photoprotective responses in cyanobacteria (1–6). OCP binds a single ketocarotenoid chromophore (1, 5), in which the 4-keto group of the β1 ionone ring is essential for its photochemical properties and functions (7). OCP photoconverts from the orange state (OCP^O) to the activated red state (OCP^R) under intense light (8). Whereas the dark reversion in vitro strongly depends on temperature (9, 10), reversion in vivo involves another small protein called fluorescence recovery protein (11). Although abundant biophysical and biochemical data suggest that OCP undergoes large conformational changes upon photoactivation, the initial photochemical events and subsequent structural changes leading up to the active state have not been established at the molecular level. The precise structural arrangements between the photoactivated OCP^R and phycobilisome have not been fully elucidated (12–14).

OCP photoactivation has been shown to involve structural changes in both the protein matrix and the ketocarotenoid chromophore (15, 16). Solution studies using size exclusion chromatography (SEC), small angle X-ray scattering (SAXS), and dynamic light scattering demonstrated that OCP exhibits increased molecular dimensions in the OCP^R state (15, 17). Native mass spectrometry combined with protein cross-linking also revealed significant domain rearrangements and a transition from dimer to monomer upon light illumination (18–20). Comparative studies of OCP^O and OCP^R using fluorescence spectroscopy, X-ray hydroxyl radical footprinting, and circular dichroism suggest a molten globule state, in which two domains of OCP are separated while retaining their secondary structures (9, 15). Structural changes in the ketocarotenoid were evidenced by 2D electronic spectroscopy and excited state dynamics probed by time-resolved absorption spectroscopy (9, 18, 21–24). Comparisons of the Raman spectra between OCP^O and various OCP^R-like states support a more planar conformation for the red-shifted ketocarotenoid, in which rotation of one or both β-ionone rings was proposed to account for the increased conjugation length (9, 17).

In contrast to extensive structural changes revealed by solution studies, the crystal structures of OCP available in the Protein Data Bank (PDB) are nearly identical in a dimeric form, despite these structures originating from different source organisms and binding chemically distinct ketocarotenoids, including echinenone (ECN), 3′-hydroxyl echinenone (3′hECN), and canthaxanthin (*SI Appendix*, Table S1). OCP consists of an all-helical N-terminal domain (NTD) and an α/β C-terminal domain (CTD) that are assembled together by three main structural elements (25) (Fig. 1 *A* and *B*). First, an N-terminal extension (NTE) (residues 1–20) packs against the central β-sheet of the CTD. Second, an extended L-shaped linker (residues 160–190) between two domains runs on the molecular surface opposite the NTE. Third, the long polyene chain of ketocarotenoid is deeply buried and bent in a tunnel that spans both domains. The linker region seems susceptible to proteolysis in vitro, resulting in two separate fragments (1). The NTD fragment alone can bind the chromophore, giving rise to red carotenoid protein (RCP) with a distinct red color. Comparisons between the crystal structures of OCP and RCP led to a recent proposal that the carotenoid undergoes a 12-Å translocation relative to the protein framework in forming

Significance

Cyanobacteria contribute to a significant portion of global solar energy acquisition via natural photosynthesis. The photosynthetic apparatus must be protected from potential molecular damages due to excess light. This work explores the photoactivation mechanism of a carotenoid-based photoreceptor involved in light harvesting regulation in cyanobacteria. Direct observations of light-induced structural changes captured in the crystal lattice at the atomic resolution suggest a light perception mechanism distinct from other well-known photoreceptors. Our findings provide structural insights into the initial molecular events as this newly characterized photoreceptor detects the light environment and triggers structural responses that reduce energy transfer from the light-harvesting antennae to the photosystems.

Author contributions: Z.R., K.-H.Z., and X.Y. designed research; S.B., Z.R., L.L., and X.Y. performed research; S.B., Z.R., L.L., X.Z., and H.S. contributed new reagents/analytic tools; S.B., Z.R., K.-H.Z., and X.Y. analyzed data; and Z.R. and X.Y. wrote the paper.

The authors declare no conflict of interest.

This article is a PNAS Direct Submission.

Data deposition: The atomic coordinates and structure factors have been deposited in the Protein Data Bank, www.pdb.org (PDB ID codes 5TUX, 5TV0, and 5TUW).

[1]To whom correspondence may be addressed. Email: xiaojing@uic.edu, zren@uic.edu, or khzhao@163.com.

[2]Present address: Institute of Hydrobiology, Chinese Academy of Sciences, Wuhan 430072, China.

This article contains supporting information online at www.pnas.org/lookup/suppl/doi:10.1073/pnas.1700956114/-/DCSupplemental.

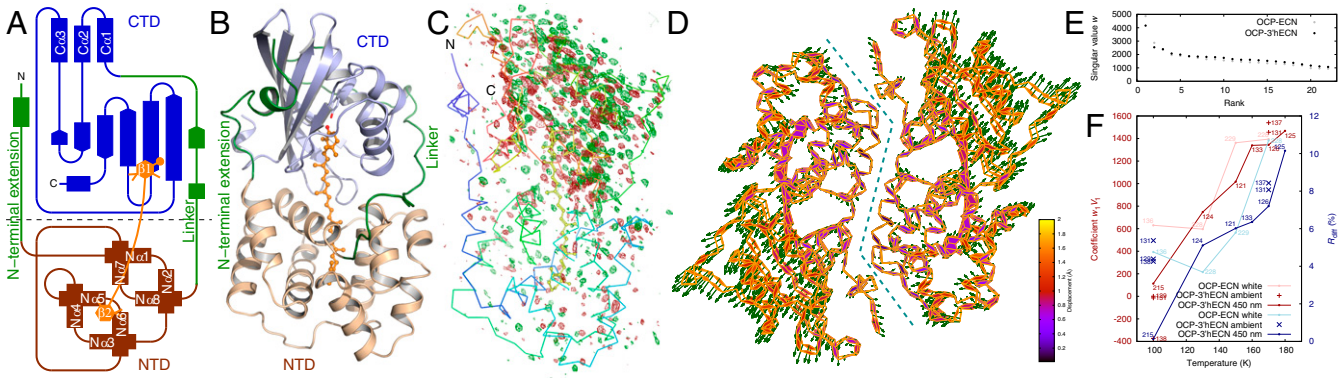

Fig. 1. Light-induced difference signals in OCP crystals. Topology (*A*) and ribbon diagrams (*B*) of the OCP structure. (*C*) The most significant component from SVD analysis of F_{Light}–F_{Dark} difference maps contoured at ±4σ in green and red, respectively. (*D*) Light-induced structural changes. Green arrows represent the directions and amplitudes of light-induced motions with 3× magnification. The dashed blue line marks the dimer interface. (*E*) The singular values w_k from SVD analysis of difference maps (OCP–ECN, gray and OCP–3′hECN, black). (*F*) Temperature dependence of the difference signals in reciprocal space (R_{diff} in blue, difference *R* factors between F_{Light} and F_{Dark}) and in real space as measured by the coefficient w_1V_1 in red. Experiments conducted under ambient light at 100 and 170 K are marked by + for the coefficients and × for R_{diff}. Crystal IDs are marked according to *SI Appendix*, Tables S3 and S4.

the photoactivated OCP^R (16). However, it is unclear what structural events trigger such drastic changes in the chromophore and its protein environment.

In this work, we use dynamic crystallography to capture light-induced structural changes in OCP crystals and have observed widespread structural changes in response to light illumination at cryogenic and room temperatures. Together with site-directed mutagenesis and spectroscopic studies, we advance a model to elucidate a sequence of chemical and structural events leading up to the activated OCP^R.

Results

Global Structural Changes. We adopt a temperature-scan (T-scan) strategy to capture light-induced structural events in the OCP crystals by examining the difference electron density maps derived from the light and dark pairwise datasets (*SI Appendix*, *SI Materials and Methods*) in two types of OCP crystals, which incorporate ECN and 3′hECN, respectively (*SI Appendix*, Tables S1 and S2). Both exhibit characteristic light-induced spectral changes from OCP^O to OCP^R in solution (*SI Appendix*, Fig. S1). We have obtained 22 F_{Light}–F_{Dark} difference electron density maps for each type of crystals, which diffracted to a resolution between 1.5 and 1.9 Å (*SI Appendix*, Tables S3 and S4). Upon visual inspection, these difference maps reveal significant and extensive map features largely consistent between two types of OCP. These difference signals in both real space and reciprocal space are clearly temperature dependent: the higher temperature at which the crystal is illuminated, the stronger the difference signals (Fig. 1*F*). Singular value decomposition (SVD) of the raw difference maps (26) and subsequent real space refinement (26) allow us to directly examine structural motions associated with the carotenoid pigment, protein secondary structures, and interfacial water molecules (Figs. 1 and 2).

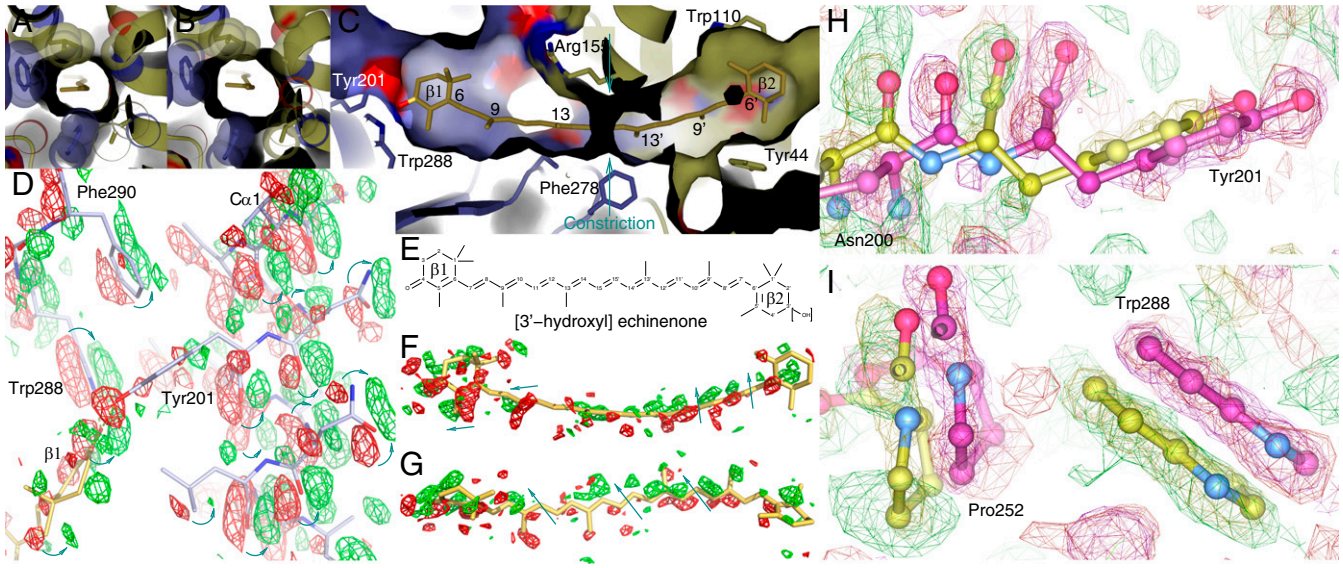

Fig. 2. Structural changes around the carotenoid binding pocket. (*A*–*C*) The ketocarotenoid tunnel spans both the CTD (blue) and the β2 ring in the NTD (yellow). The narrow constriction (*A*) widens upon light activation (*B*) as viewed from the left of *C* along the tunnel. (*D*) F_{Light}–F_{Dark} difference map (contoured at ±4σ) of OCP–ECN around the β1 ionone ring and helix Cα1. Blue arrows indicate motions from the negative (red) to the positive (green) densities. (*E*) Chemical structures of echinenone (ECN) and 3′-hydroxyl echinenone (3′hECN). (*F* and *G*) Difference electron densities associated with the chromophore in two orthogonal views. (*H* and *I*) Structural changes at Tyr201 and Trp288 (light, magenta and dark, yellow). The observed (green and red mesh) and calculated (yellow and magenta mesh) positive and negative electron densities are compared to demonstrate the goodness of real space refinement (26).

Overall, the difference densities are more pronounced in the CTD than in the NTD (Fig. 1*C*). In the OCP dimer, the difference signals are stronger in regions farther away from the dimer interface. The structural changes are highly similar in the crystals of OCP–ECN and OCP–3′hECN (Fig. 1*F* and *SI Appendix*, Fig. S3). In contrast to the small-amplitude movement in the NTD (<0.8 Å; Fig. 1*F* and *SI Appendix*, Fig. S3*A*), the CTD undergoes significant atomic displacements (as large as 2 Å) in a direction away from the NTD and the dimer interface. The NTE is packed against the β-sheet of the CTD via largely hydrophobic interactions (*SI Appendix*, Fig. S4*B*), while forming extensive hydrogen bonds with the NTD of the partner subunit across the dimer interface (*SI Appendix*, Fig. S4*A*). Only weak difference electron densities are observed in the NTE (Fig. 1*C*), suggesting that the NTE is torn apart from the departing CTD of the same subunit, while tightly associated with the NTD of the partner subunit (Fig. 1*F* and *SI Appendix*, Fig. S3). These motions may lead to a partial domain separation in the crystal lattice along with molecular expansion for OCP both as monomer and dimer (Fig. 1*D*).

Structural Changes in Carotenoid Binding Pocket. Compared with other carotenoid binding proteins (16, 27), the ketocarotenoid is significantly bent and twisted inside a tunnel spanning both domains in the OCP structure (Fig. 2 and *SI Appendix*, Fig. S5). The accumulative angle off the π-conjugation plane in the polyene chain is ∼36°. The ketocarotenoid is kinked around the C13′ position near the domain interface. The protein–pigment interactions are very different around the β-ionone rings. In the CTD, the ketocarotenoid is located in a rather ample pocket filled with water molecules lining around the hydrophobic chain between C9 and C13 (*SI Appendix*, Figs. S6*A* and S7 *A* and *B*). The β1 ionone ring is largely surrounded by hydrophobic residues except Tyr201 and Trp288 (equivalent to Tyr203 and Trp290 in *Arthrospira maxima* and *Anabaena*), which tether the β1 ring at the 4-keto group with two strong hydrogen bonds of 2.6 and 2.9 Å, respectively (Fig. 2). The β1 ring is tilted relative to the π-conjugation plane with a rotation angle about C6–C7 of 53°. The carotenoid tunnel gets tighter in the NTD with a bottleneck near the domain interface constricting the polyene chain (Fig. 2 *A*–*C* and *SI Appendix*, Fig. S6*B*). Residues from both domains pinch onto the mid segment of the carotenoid from all directions via close van der Waals interactions (*SI Appendix*, Fig. S6*B*). The β2 ring buried inside the NTD is surrounded by bulky residues in a protein environment largely devoid of water molecules. Specifically, the β2 ring forms stacking interactions with the indole ring of Trp110 in an orientation defined by a rotation angle of ∼69° about the C6′–C7′ single bond (Fig. 2*C* and *SI Appendix*, Fig. S6*C*).

Both the raw and SVD-filtered difference maps show evenly spaced positive and negative difference densities associated with the carotenoid, suggesting a small shift roughly along the conjugated plane of the polyene chain (Fig. 2 *F* and *G*). Three helices (Cα1–3) and the central β-sheet of the CTD move together like a rigid body away from the NTD and the dimer interface. In the helix Cα1 (residues 196–207) where Tyr201 is located (Fig. 1 *A* and *B*), pairwise positive and negative densities that sandwich the peptide planes and bulky side chains clearly show the concerted motions of Cα1 (Fig. 2*D*), in which Tyr201 moves in the plane of its aromatic side chain (Fig. 2 *D* and *H*). Concomitantly, Trp288 from the β-sheet also moves in concert with two slabs of positive and negative densities around its indole ring (Fig. 2 *D* and *I*). The nearby Phe290 moves accordingly (Fig. 2*D*). As a result, the hydrogen bonds from the 4-keto group to Tyr201 and Trp288 are longer by 0.2–0.4 Å in the refined light structures of OCP–ECN and OCP–3′hECN. This trend is likely to develop further in solution where hindrance from the crystal lattice is absent.

Strong difference electron densities extend to the domain interface where the ring of constriction seems loosened up when Trp277 and Phe278 move away with the CTD, whereas Leu107 and Arg155 stay with the NTD (Fig. 2 *A* and *B*). We have also observed movements associated with water molecules at the dimer interface where a network of hydrogen bonds and the Arg155–Glu244 salt bridge are altered (*SI Appendix*, Fig. S7 *C* and *D*). These changes at the domain interface may also account for increased solvent accessibility near the cluster of Pro276–Trp277–Phe278 in the activated OCP (15). In the NTD, the difference densities are either clustered near the CTD or on the outer surface of the OCP dimer (Fig. 1*C*). The indole ring of Trp110 appears to move together with the β2 ring. The enhanced Trp fluorescence signal associated with OCP^R is likely to arise from separation of Trp277 and Trp288 from the ketocarotenoid. Taken together, these observations indicate an enlargement of the carotenoid-binding pocket (Fig. 2), which permits relaxation of the strained ketocarotenoid.

Single-Crystal Microspectrometry. To examine the photoactivity in the crystalline state, we measured the absorption spectra from solutions and the single crystals of OCP using a microspectrophotometer developed in our laboratory. The $OCP^O \rightarrow OCP^R$ photoconversion can be readily detected in solution (Fig. 3*A*). Confirming previous reports, we also observe that OCP in solution can be degraded to form RCP (1, 16) if the sample is placed under light for an extended period (3–5 d) at room temperature (*SI Appendix*, Fig. S8*A*). However, we did not observe any clear spectral changes in the single crystals of both OCP–ECN and OCP–3′hECN using the same experimental setup (Fig. 3*B*). The crystal spectra of OCP exhibit a slightly red-shifted absorption band around 500 nm corresponding to the $S_0 \rightarrow S_2$ transition of carotenoids (28). To avoid unwanted photoactivation,

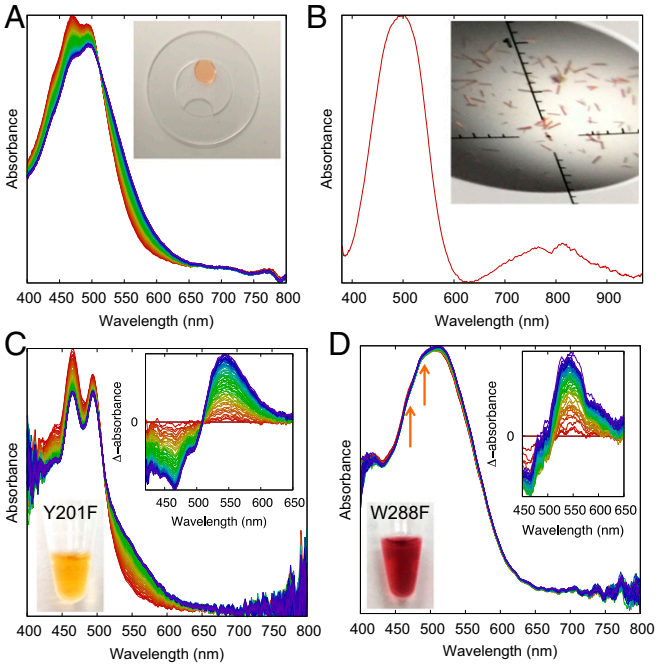

Fig. 3. Absorption spectra of OCP in solution and single crystals. (*A*) Time-resolved absorption spectra of OCP–ECN solution under flooded white light illumination during a 90-s recording are plotted from red to blue in equal time interval. Fresh protein solution at the concentration of 3 mg/mL and the reference buffer (clear drop) are loaded into a device (*Inset*). (*B*) The single-crystal OCP–ECN shows no detectable light-induced spectral change. (*C*) Time-resolved absorption spectra of the Y201F mutant in solution during a 60-s recording under filtered white light (shortpass filter <600 nm), plotted in equal time interval from red to blue (*Inset*: difference absorbance with respect to the first curve). (*D*) Time-resolved absorption spectra of the W288F mutant. Two small shoulders marked by the orange arrows suggest a small fraction of the orange state undergoing photoconversion (*Inset*).

dim safety light with a longpass filter (>600 nm) was used to align crystals. We also measured the absorption spectrum of the protein sample from dissolved OCP crystals, which showed the dual-peak spectrum characteristic of OCP^O (*SI Appendix*, Fig. S8*B*) indicating the protein integrity in crystals. Another evidence supporting that the OCP crystals indeed adopt the OCP^O state comes from the Y44S mutant (PDB ID 3MG2), which is locked in the OCP^O state (*SI Appendix*, Fig. S8*C*) (29), and differs very little from the wild-type structure (*SI Appendix*, Table S1).

Light-induced spectral change is often used as an indicator for photoactivity in crystals. However, the absence of spectral changes does not rule out photoactivity or existence of any spectroscopically silent structural changes. A good example is the UV-B photoreceptor from plant UVR8, which does not show any detectable light-induced absorption spectral changes in a steady-state experiment, but undergoes UV-B–induced dimer dissociation resulting in visible cracks in crystals (30). We postulate that the spectral change of OCP observed in solution is the consequence rather than the cause of light-induced conformational changes (9, 17). Lack of spectral changes in OCP crystals is attributed to the lattice constraint that prohibits large structural changes required for the completion of photoactivation (Fig. 4 *A*–*D*). The crystal lattice may also be responsible for the slightly red-shifted crystal spectra, similar to thermal effects at cryogenic temperature (31).

The crystal spectra lack the fine vibrational features exhibited in the solution spectra, but they consistently show an additional absorption band at longer wavelengths at 650–950 nm (Fig. 3*B*). Similar features have been experimentally observed for carotenoids in the ultrafast time regime (fs–ps) by transient absorption spectroscopy (32). The physical origin for the presence or absence of the fine spectral features and the S_1 band in carotenoids require further investigation. Our high-resolution crystal structures accompanied with absorption spectra of single crystals would be highly informative for quantum mechanics calculations and other studies.

Photoactivation Mechanism. It has been also proposed that the first step in OCP photoactivation involves a rotation of the β-ionone ring about the C6–C7 single bond in the CTD (9). However, our observations do not support significant rotational motions in both β-ionone rings nor a photoisomerization event as observed for retinal in rhodopsins (33). Instead, the difference electron densities suggest a small displacement of the carotenoid mostly in the plane of the polyene chain (Fig. 2 *F* and *G*). In all difference maps, the pronounced difference densities appear to emanate from the β1 ring, suggesting an epicenter constituted by three distinct structural moieties: the carbonyl group of β1, Tyr201, and Trp288 of the CTD (Fig. 1*C*). It has been shown that modifications to this tripartite structure significantly affect the OCP photoactivity. It was reported that OCP bound with zeaxanthin lacking the 4-keto group is unable to photoconvert (7). The single mutants such as Y201H, Y201S, W288H, and W288S altered carotenoid selectivity and/or photoconversion when overexpressed in *Synechocystis* strains lacking zeaxanthin and 3′hECN (34). To examine the individual role(s) of Tyr201 and Trp288, we made two additional single mutants, Y201F and W288F. In our coexpression *Escherichia coli* system, Y201F clearly favors β-carotene over ECN, evidenced by the bright yellow color and characteristic spectral features (Fig. 3*C*). It appears that a certain population of Y201F still binds ECN, hence, able to photoconvert to OCP^R. The reddish W288F seems to retain the high affinity for ECN, but it exhibits an OCP^R-like absorption spectrum (Fig. 3*D* and *SI Appendix*, Fig. S8*D*). We postulate that Tyr201 promotes chromophore selectivity, whereas Trp288 is important for stabilizing the OCP^O state.

In the OCP^O structure, the orientations of the β-rings are largely dictated by protein–pigment interactions, whereas the polyene chain is twisted and tightly constricted at the domain interface. We reason that such a highly strained conformation of ketocarotenoid must be loaded with a bending moment or tension (Fig. 2*C*), which may be sustained by the sideway hydrogen bond between the 4-keto group and Trp288 (Fig. 4*E*). The single hydrogen bond to Tyr201 along the polyene chain would allow more flexibility for the ketocarotenoid leading to an OCP^R-like state in W288F (Fig. 3*D*) or W288A, which persistently quenches the phycobilisome fluorescence (17, 35). Similarly, weakened hydrogen bonds in the tripartite structure may also explain the chemical activation of OCP by kosmotropes (36).

Taken together, we hypothesize that the photoactivation of OCP originates in the conjugated carbonyl group in the β1 ring of the ketocarotenoid. The resulting shift in keto–enol equilibrium weakens or disrupts the hydrogen bonds between the β1 ring and the protein moiety (Fig. 4*F*), which allows the ketocarotenoid to relax inside the protein tunnel, thereby providing the initial driving force for domain separation (Fig. 4*C*). As two domains further separate, the polyene chain also loosens up at the domain interface (Fig. 2 *A*–*C*). Eventually, the bending moment sustained in the long polyene chain eases off, and the relaxed chromophore adopts a more planar conformation in a less rigid protein framework leading to the formation of the OCP^R state.

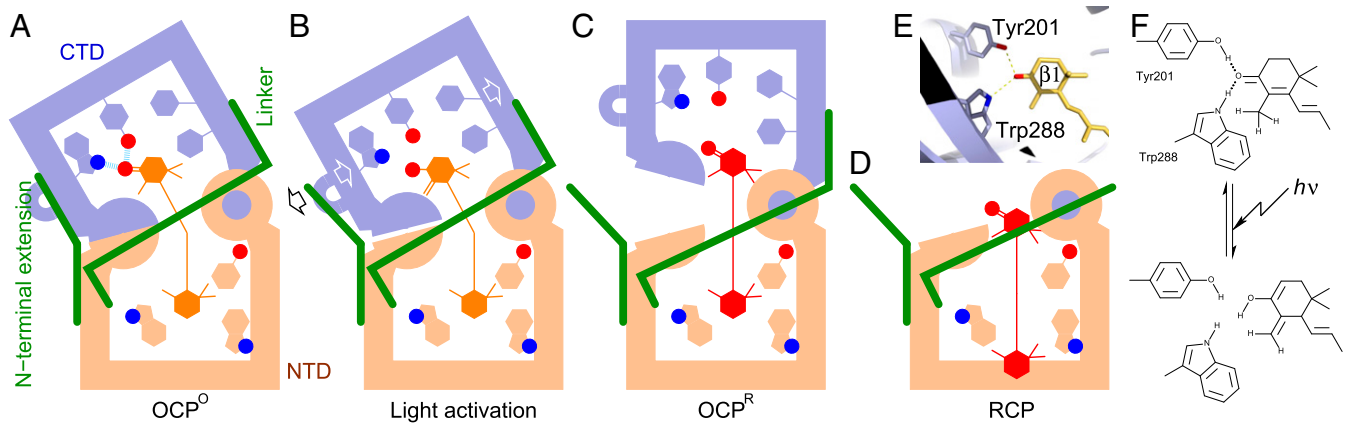

Fig. 4. A model for OCP photoactivation. (*A*) The bent ketocarotenoid is embedded in the OCP^O structure where two protein domains are tightly coupled. (*B*) Light activation disrupts the pigment–protein interactions at the β1 end of the chromophore, leading to partial domain separation as well as detachment of the NTE from the CTD. (*C*) Subsequent protein structural changes accompany relaxation of the carotenoid that adopts a more planar conformation in OCP^R. (*D*) The carotenoid may undergo further translocation as in RCP. Short hydrogen bonds between Trp288/Tyr201 and the β1 ionone ring (*E*) may be disrupted by a transient shift in keto–enol equilibrium (*F*) due to light excitation of the conjugated carbonyl group in the β1 ring.

Discussion

Primary Photo Events. This work presents a light perception mechanism distinct from other known photoreceptors (37). We propose that the initial photochemical event in OCP originates in the essential conjugated carbonyl group of the β1 ring, where a light-induced shift in keto–enol equilibrium weakens the interactions between the chromophore and protein moiety. Similar to other photoreceptors (33, 38), subsequent protein structural changes in OCP are driven by thermal relaxation of the strained chromophore in a confined protein cavity. However, a key difference is that the strain energy is preloaded in a distorted ketocarotenoid in the OCP^O structure, whereas the initial conformational strain arises from photoisomerization in phytochromes and rhodopsins (33, 38).

The proposed enolization mechanism implies an sp2→sp3 orbital transition at the C6 position of the carotenoid (Fig. 4*F*), which is not directly observed in our difference maps. It is likely that such hybrid orbital transition is short lived even at low temperatures beyond the accessible time scales of our data collection protocol. Rapid time-resolved techniques of spectroscopy and crystallography are needed to detect such transient species on the ultrafast time scale (39). However, we did observe a small shift in the ketocarotenoid with a subtle rotation in the β1 ring about the C6–C7 bond (9) (Figs. 1 and 2). The more planar conformation of ketocarotenoid in the OCP^R state is supported by the enhanced signals for C=C stretch together with the reduced hydrogen-out-of-plane mode detected by Raman spectroscopy (17).

The role of bulky residues such as Tyr44 and Trp110 surrounding the β2 ring seems to be different from those of Tyr201 and Trp288 in the CTD (34). Whereas the Y44F and W110F mutants behave just like the wild type, Y44S and W110S are unable to photoconvert from OCP^O to OCP^R (*SI Appendix*, Fig. S8*C*), except that photoactivation of W110S may occur at a higher temperature of 30 °C (29, 34). The bulky residues around the β2 ionone ring are expected to render significant holding power on the chromophore as it becomes straight upon photoactivation. So the NTD would win a tug of war in wild-type OCP as well as Y44F and W110F mutants (34), as the departing CTD pulls on the chromophore at the other end. In contrast, the chromophore is let go by the NTD in the Y44S and W110S mutants because the interactions with the β2 ring are significantly weaker. A tighter grip on the chromophore seems to be important for decoupling the CTD from the chromophore, a critical event during photoactivation (Fig. 4*F*).

Domain Separation and Spectral Red Shift. Joint analysis of the OCP structures suggests that the internal protein framework of the CTD is rather rigid compared with the NTD (*SI Appendix*, Fig. S9). The relative orientation between the two four-helix bundles in the NTD varies among the OCP structures (*SI Appendix*, Fig. S9*A*). These helical bundles are significantly rearranged to accommodate the translocated carotenoid as in the RCP structure (*SI Appendix*, Fig. S10) (16). However, the observed rigid-body motion of the CTD does not contradict the internal rigidity of the domain. In addition, the amplitudes of light-induced structural changes seem to bear little correlation with the B-factor distribution of the OCP structure (Fig. 1*F* and *SI Appendix*, Fig. S11*A*), suggesting that the observed motions do not arise from the intrinsic thermal fluctuations or static structural disorders in crystal lattice.

A molten globule state for OCP^R has been suggested by various solution studies, in which large conformational changes of OCP appear to require little changes in its secondary structure composition (9, 15). OCP^R exhibits similar hydrodynamic behaviors as apo-OCP as they appear to comigrate on a sizing column faster than OCP^O (*SI Appendix*, Fig. S1). Attempts to crystallize the OCP^R or apo-OCP have not been successful. Interestingly, we observed that some extremely thin reddish crystals of OCP curled up in the crystallization drops after an extended exposure to room light. Such changes in crystal morphology may be resulted from structural changes with an angular component consistently lined up in crystals permitted by mechanically fragile thin crystals (*SI Appendix*, Fig. S12*C*).

The overall shape and fine structure of the absorption spectrum of a carotenoid depend on the extent of planarity it can achieve. Generally speaking, λ_{max} increases with the overall length of the conjugated system in a chromophore (40). Compared with RCP and other carotenoid binding proteins (16, 41), the ketocarotenoid in the OCP^O structure adopts a highly distorted conjugation system. In addition to the curved polyene chain, C6–C7 single bond is in the *anti*-conformation, which sets the C5=C6 double bond in the β1 ring off the conjugation plane of the polyene chain by 53° compared with 34° in the RCP structure (16). Similarly, the corresponding torsion angles of C6′–C7′ around the β2 ring are 69° in OCP versus 40° in RCP except that the C6′–C7′ single bond is in the *syn*-conformation (Fig. 2*E*). It is plausible that photoactivation of OCP allows the chromophore to restore a more extended conjugated system, hence a red-shifted λ_{max}.

The activated OCP is presumed to significantly expand in solution (15). However, it remains to be seen whether such dramatic molecular expansion involves the proposed 12-Å translocation of the ketocarotenoid into the NTD (16), and how back translocation would occur to achieve fast dark reversion (9). X-ray footprinting experiments do not seem to support a vacated CTD in OCP^R, in which those residues lining the binding pocket would experience large changes in solvent accessibility (15). We postulate that instead of full retraction from the CTD, the ketocarotenoid adopts a relaxed, more planar conformation in a much-expanded tunnel inside the protein framework (Fig. 4*C*) (9, 23).

N-Terminal Extension and Dimerization. The oligomeric state of OCP in vitro depends on the protein concentration as well as the detection method. Whereas SEC and SAXS data show monomeric OCP in dilute solution (<1 mg/mL; *SI Appendix*, Fig. S1) (15), native mass spectroscopy suggested a light-triggered dimer-to-monomer transition (18). In addition, the same dimeric assembly has been found in all OCP crystal structures determined so far (*SI Appendix*, Table S1). But the oligomeric state of OCP in its native environment has not been established. We predict that the OCP dimer as in the crystal lattice may dissociate if the observed partial domain separation is allowed to fully develop in solution. The *trans*-association between the NTE and NTD of the partner subunit at the dimer interface appears to be tighter than the *cis*-association within a subunit (Fig. 1 and *SI Appendix*, Figs. S3 and S4). It is plausible that two partner subunits lend each other a hand to detach the NTE from the CTD. In other words, the NTE may function as a latch, which tightly couples two protein domains and maintains the ketocarotenoid conformation in OCP^O (Fig. 4). OCP lacking the NTE was reported to migrate as two separate fractions in SEC (42) with a purple fraction showing the absorption spectrum similar to that of the W288A mutant (35) and OCP^R. We speculate that the absence of the NTE or detachment of the NTE from the CTD as observed would facilitate domain separation and OCP activation, which is consistent with increased solvent accessibility in the NTE and the first helix Nα1 of the illuminated OCP in solution (15).

Dynamic Crystallography. Dynamic crystallography aims to capture structural changes in response to a physical or chemical perturbation. However, such structural changes in crystal are often so small in amplitude and low in population that they elude an electron density map dominated by the unperturbed species. The difference Fourier method is needed to directly examine structural differences between the perturbed and reference states. Although this difference method is particularly sensitive to subtle signals, it is also highly susceptible to variations from crystal to crystal. It is thus extremely important to acquire difference signals from different segments of the same crystal whenever possible. Given the rod shape of OCP crystals, we were able to collect both

the dark and light datasets from separate segments of the same crystal to achieve the best difference signals and to avoid possible effects due to X-ray radiation damage. This T-scan strategy has unraveled remarkable light-induced structural changes in other photoreceptors such as bacteriophytochrome and UVR8 (30, 38). These results demonstrate that it is entirely possible to capture large-scale structural motions in the crystal lattice when a photoactive crystal is illuminated at cryogenic temperatures near the glass transition temperature (30, 43).

It is noteworthy that the R_{diff} values between the light and dark datasets are very small (3–10%). R_{diff} are comparable to the corresponding R_{merge} values (*SI Appendix*, Tables S3 and S4), supporting the overall agreement and isomorphism between the paired datasets. Widespread difference electron densities across the entire molecule and small difference between light and dark datasets suggest that only a small fraction of the molecules in crystals are photoconverted. Such limited extent of photoconversion warrants good isomorphism between the light and reference datasets thereby giving rise to accurate measurements of widespread yet subtle differences as observed in this work. We must point out that light-induced structural changes captured in the crystal lattice do not directly represent the OCP^R state in solution. These high-resolution difference signals, although broad in scope, are small in amplitude and spectroscopically silent (Fig. 3*B*). The crystal lattice evidently imposes an energy barrier that hinders further development of larger conformational changes required for the full activation of OCP. On the other hand, such lattice constraint and cryogenic temperature offer an invaluable kinetic trap for crystallographic observations of those structural events too unstable to capture at room temperature (30, 38, 43).

Materials and Methods

OCP–ECN and OCP–3′hECN were purified from a modified coexpression system in *E. coli* (44) and *Synechocystis* PCC 6803, respectively (*SI Appendix, SI Materials and Methods*). Difference Fourier maps between the pairwise light and reference datasets were calculated to examine light-induced structural changes at different temperatures. These difference maps were then jointly analyzed by SVD. The dark and light structures were refined against the SVD-filtered difference maps in real space (26). An overall workflow of the dynamic crystallography method is shown in *SI Appendix*, Fig. S2. Extensive details of the data collection and analysis for all methods are provided in *SI Appendix, SI Materials and Methods*.

ACKNOWLEDGMENTS. We thank the staff at Life Sciences Collaborative Access Team (LS-CAT) for support in X-ray diffraction data collection. Use of the LS-CAT Sector 21 was supported by the Michigan Economic Development Corporation and the Michigan Technology Tri-Corridor (Grant 085P1000817). Use of the Advanced Photon Source was supported by the US Department of Energy, Office of Science, Office of Basic Energy Sciences, under Contract DE-AC02-06CH11357. This work is supported by grants from the University of Illinois at Chicago and National Institutes of Health (R01EY024363 to X.Y.) and from National Natural Science Foundation of China (21472055 to K.-H.Z.).

1. Wu YP, Krogmann DW (1997) The orange carotenoid protein of *Synechocystis* PCC 68031. *Biochim Biophys Acta* 1322:1–7.
2. Wilson A, et al. (2006) A soluble carotenoid protein involved in phycobilisome-related energy dissipation in cyanobacteria. *Plant Cell* 18:992–1007.
3. Kirilovsky D (2007) Photoprotection in cyanobacteria: The orange carotenoid protein (OCP)-related non-photochemical-quenching mechanism. *Photosynth Res* 93:7–16.
4. Bailey S, Grossman A (2008) Photoprotection in cyanobacteria: Regulation of light harvesting. *Photochem Photobiol* 84:1410–1420.
5. Kirilovsky D, Kerfeld CA (2012) The orange carotenoid protein in photoprotection of photosystem II in cyanobacteria. *Biochim Biophys Acta* 1817:158–166.
6. Mach J (2014) Orange carotenoid protein quenches excess energy and singlet oxygen. *Plant Cell* 26:1380.
7. Punginelli C, Wilson A, Routaboul J-M, Kirilovsky D (2009) Influence of zeaxanthin and echinenone binding on the activity of the Orange Carotenoid Protein. *Biochim Biophys Acta* 1787:280–288.
8. Kirilovsky D, Kerfeld CA (2016) Cyanobacterial photoprotection by the orange carotenoid protein. *Nat Plants* 2:16180.
9. Maksimov EG, et al. (2015) The signaling state of orange carotenoid protein. *Biophys J* 109:595–607.
10. Wilson A, et al. (2008) A photoactive carotenoid protein acting as light intensity sensor. *Proc Natl Acad Sci USA* 105:12075–12080.
11. Sutter M, et al. (2013) Crystal structure of the FRP and identification of the active site for modulation of OCP-mediated photoprotection in cyanobacteria. *Proc Natl Acad Sci USA* 110:10022–10027.
12. Berera R, et al. (2012) The photophysics of the orange carotenoid protein, a light-powered molecular switch. *J Phys Chem B* 116:2568–2574.
13. Harris D, et al. (2016) Orange carotenoid protein burrows into the phycobilisome to provide photoprotection. *Proc Natl Acad Sci USA* 113:E1655–E1662.
14. Kirilovsky D, Kerfeld CA (2013) The Orange Carotenoid Protein: A blue-green light photoactive protein. *Photochem Photobiol Sci* 12:1135–1143.
15. Gupta S, et al. (2015) Local and global structural drivers for the photoactivation of the orange carotenoid protein. *Proc Natl Acad Sci USA* 112:E5567–E5574.
16. Leverenz RL, et al. (2015) PHOTOSYNTHESIS. A 12 Å carotenoid translocation in a photoswitch associated with cyanobacterial photoprotection. *Science* 348:1463–1466.
17. Maksimov EG, et al. (2016) A comparative study of three signaling forms of the orange carotenoid protein. *Photosynth Res* 130:389–401.
18. Zhang H, et al. (2014) Molecular mechanism of photoactivation and structural location of the cyanobacterial orange carotenoid protein. *Biochemistry* 53:13–19.
19. Liu H, et al. (2014) Mass spectrometry footprinting reveals the structural rearrangements of cyanobacterial orange carotenoid protein upon light activation. *Biochim Biophys Acta* 1837:1955–1963.
20. Liu H, et al. (2016) Dramatic domain rearrangements of the cyanobacterial orange carotenoid protein upon photoactivation. *Biochemistry* 55:1003–1009.
21. Liu W-L, Wang Z-G, Zheng Z-R, Li A-H, Su W-H (2008) Effect of β-ring rotation on the structures and vibrational spectra of β-carotene: Density functional theory analysis. *J Phys Chem A* 112:10580–10585.
22. Chábera P, Durchan M, Shih PM, Kerfeld CA, Polívka T (2011) Excited-state properties of the 16 kDa red carotenoid protein from *Arthrospira maxima*. *Biochim Biophys Acta* 1807:30–35.
23. De Re E, et al. (2014) Insights into the structural changes occurring upon photoconversion in the orange carotenoid protein from broadband two-dimensional electronic spectroscopy. *J Phys Chem B* 118:5382–5389.
24. Šlouf V, et al. (2017) Ultrafast spectroscopy tracks carotenoid configurations in the orange and red carotenoid proteins from cyanobacteria. *Photosynth Res* 131:105–117.
25. Kerfeld CA, et al. (2003) The crystal structure of a cyanobacterial water-soluble carotenoid binding protein. *Structure* 11:55–65.
26. Ren Z, et al. (2013) Resolution of structural heterogeneity in dynamic crystallography. *Acta Crystallogr D Biol Crystallogr* 69:946–959.
27. Luecke H, et al. (2008) Crystallographic structure of xanthorhodopsin, the light-driven proton pump with a dual chromophore. *Proc Natl Acad Sci USA* 105:16561–16565.
28. Balevičius V, Jr, Abramavicius D, Polívka T, Galestian Pour A, Hauer J (2016) A unified picture of S* in carotenoids. *J Phys Chem Lett* 7:3347–3352.
29. Wilson A, et al. (2010) Structural determinants underlying photoprotection in the photoactive orange carotenoid protein of cyanobacteria. *J Biol Chem* 285:18364–18375.
30. Zeng X, et al. (2015) Dynamic crystallography reveals early signalling events in ultraviolet photoreceptor UVR8. *Nat Plants* 1:pii: 14006.
31. Niedzwiedzki DM, Liu H, Blankenship RE (2014) Excited state properties of 3′-hydroxyechinenone in solvents and in the orange carotenoid protein from Synechocystis sp. PCC 6803. *J Phys Chem B* 118:6141–6149.
32. Polívka T, Herek JL, Zigmantas D, Åkerlund H-E, Sundström V (1999) Direct observation of the (forbidden) S1 state in carotenoids. *Proc Natl Acad Sci USA* 96:4914–4917.
33. Lutz I, et al. (2001) Primary reactions of sensory rhodopsins. *Proc Natl Acad Sci USA* 98:962–967.
34. Wilson A, Punginelli C, Couturier M, Perreau F, Kirilovsky D (2011) Essential role of two tyrosines and two tryptophans on the photoprotection activity of the Orange Carotenoid Protein. *Biochim Biophys Acta* 1807:293–301.
35. Sluchanko NN, et al. (2017) The purple Trp288Ala mutant of *Synechocystis* OCP persistently quenches phycobilisome fluorescence and tightly interacts with FRP. *Biochim Biophys Acta* 1858:1–11.
36. King JD, Liu H, He G, Orf GS, Blankenship RE (2014) Chemical activation of the cyanobacterial orange carotenoid protein. *FEBS Lett* 588:4561–4565.
37. Möglich A, Yang X, Ayers RA, Moffat K (2010) Structure and function of plant photoreceptors. *Annu Rev Plant Biol* 61:21–47.
38. Yang X, Ren Z, Kuk J, Moffat K (2011) Temperature-scan cryocrystallography reveals reaction intermediates in bacteriophytochrome. *Nature* 479:428–432.
39. Moffat K (2001) Time-resolved biochemical crystallography: A mechanistic perspective. *Chem Rev* 101:1569–1581.
40. Britton DG, Young AJ (1993) *Methods for the Isolation and Analysis of Carotenoids. Carotenoids in Photosynthesis* (Springer Netherland, Dordrecht, The Netherlands), pp 409–457.
41. Melnicki MR, et al. (2016) Structure, diversity, and evolution of a new family of soluble carotenoid-binding proteins in cyanobacteria. *Mol Plant* 9:1379–1394.
42. Sluchanko NN, Slonimskiy YB, Moldenhauer M, Friedrich T, Maksimov EG (May 15, 2017) Deletion of the short N-terminal extension in OCP reveals the main site for the FRP binding. *FEBS Lett*, 10.1002/1873-3468.12680.
43. Ringe D, Petsko GA (2003) The 'glass transition' in protein dynamics: What it is, why it occurs, and how to exploit it. *Biophys Chem* 105:667–680.
44. Cunningham FX, Jr, et al. (1996) Functional analysis of the beta and epsilon lycopene cyclase enzymes of Arabidopsis reveals a mechanism for control of cyclic carotenoid formation. *Plant Cell* 8:1613–1626.